Hindawi
Advances in Civil Engineering
Volume 2024, Article ID 5548837, 17 pages
https://doi.org/10.1155/2024/5548837

Research Article

Analysis of Dynamic Evolution of Surrounding Rock Movement and Stress-Fracture in the Upward and Repeated Mining of Close-Distance Coal Seams

Ningbo Peng,[1] **Chunlei Zhang**,[1] **Ruimin Feng**,[2] **Arifuggaman Arif**,[1] **Xi Chen**,[1] **Weidong Zhang**,[1] **Shuai Zhang**,[3] **and Mingjie Feng**[1]

[1]*Faculty of Architecture and Civil Engineering, Huaiyin Institute of Technology, Huai'an, Jiangsu 223001, China*
[2]*Department of Civil Engineering, University of Arkansas, Fayetteville, AR 72701, USA*
[3]*School of Civil Engineering, Beijing Jiaotong University, Beijing 100044, China*

Correspondence should be addressed to Chunlei Zhang; fangyuanleihua@126.com

Received 24 November 2023; Revised 28 December 2023; Accepted 29 December 2023; Published 28 February 2024

Academic Editor: Chu Zhaofei

The distribution of mining-induced stress and the resulting rock fractures are two crucial factors affecting mineral extraction in protective layer mining. This research establishes a correlation between the vertical fracture aperture and the second derivative of the rock layer's subsidence curve equation. The article explores the span requirement for a simply supported beam to fracture. This condition is relevant to understanding the dynamic evolution of rock movement and stress fractures during repeated mining of close-distance coal seams. Our study investigates alterations in rock stress and fractures resulting from repeated upward mining of coal seams, using the nearby coal seam cluster in Jincheng Mine as a case study. The research findings indicate that during the mining of the upper coal seam, the roof experiences significant but brief periodic loading intervals, as well as severe and moderate periodic loading. As mining progresses to the lower coal seam, pressure relief of the upper coal seam gradually increases in both degree and range. In the upper coal seam, the vertical stress distribution follows a sequence of "V," "U," and "W" forms. The upper coal seam undergoes five stages of expansion deformation: compression, expansion, increased expansion, decreased expansion, and stable expansion.

1. Introduction

Mining-induced fractures in the surrounding rock are channels for gas diffusion and accumulation. Studying the dynamic evolution law of surrounding rock fractures during mining has important basic significance for improving gas extraction systems and preventing gas disasters [1–3]. After protective layer mining, the stress balance state of the surrounding rock is disrupted, and the rock layers of the roof and floor of the coal seam begin to move and rupture toward the gob, causing the overlying rock stress to redistribute gradually [4]. Within the unloading range of the roof and floor of the protective layer, the protected layer undergoes expansion deformation, and horizontal and vertical fractures gradually develop until they are connected to the gob of the protected layer [5]. During the continuous extraction process of the protective layer, the displacement field, stress field, and fracture field caused by mining exhibit dynamic changes, and it has been studied by many scholars. Qian et al. [6–9] proposed the key layer theory based on the model of "voussoir beam structure" in the overlying rock layer of a longwall working face, revealing the "O"-shaped crack circle characteristics of mining-induced fractures. Yuan [10] and Lu et al. [11] proposed the concept of "roof annular cracks" and believed that there is a "vertical crack development zone" on the gob side. Li and Lin [12] and Lin et al. [13] proposed the "mining-induced fissure elliptic paraboloid zone" and "mining-induced fissure round-rectangle trapezoidal zone." Xie et al. [14] and Yu et al. [15] revealed the fractal characteristics of mining-induced fractures in the overlying rock layer of a working face through physical simulation experiments and obtained the statistical relationship between the fractal dimension of fracture distribution and mining space.

Most of the above studies were based on single coal seam mining conditions, and there are few reports on the study of surrounding rock movement and fracture development and redevelopment under the conditions of repeated mining of multiple coal seams.

China's coal mining operations are progressively extending to greater depths, leading to the prevalence of deep coal seams [16]. The displacement, stress, and fracture fields resulting from mining activity may exhibit significant variations when multiple protective layers are influenced by mining, as compared to single protective layer mining [17, 18]. Hence, investigating the evolution laws governing the displacement, stress, and fracture fields during the mining of numerous protective layers in coal seam groups, as well as the extent of pressure protection provided by the protected layer, holds paramount importance. Wu et al. [19] developed a calculation method to determine the spatial distribution of fractures introduced by mining in the rock layer above. They conducted simulation experiments to investigate the distribution of fracture rates in both vertical and horizontal directions after repeated coal seam mining. Through these experiments, they obtained a quantitative description of the fractures induced by mining in the rock layer above. Li et al. [20] examined the occurrence of rock failure in the underlying strata when numerous coal seams were repeatedly mined. Lin et al. [21] examined the properties of cracks in the rock layer above coal seams following many mining operations and elucidated the evolutionary pattern of gas storage and transport zones. These studies have laid the groundwork for subsequent investigations into the dynamic evolution rules of surrounding rock movement and fracture formation during the repeated mining of coal seams. This paper further explores the laws governing the movement of surrounding rock and the development of fractures during repeated mining of closely spaced coal seam groups. Building upon previous research, this study is conducted in the context of a coal mine in Jincheng with the aim of establishing a theoretical foundation for determining optimal timing and locations for gas extraction.

The primary focus of the coal mine is the extraction of the No. 3 coal seam, which possesses a straightforward geological composition and an average thickness of approximately 5.58 m. As the mine expands toward the west, the burial depth gradually increases, leading to the gas content and the quantity of gas emissions. The initial gas concentration in the mining area of the fourth mining panel is relatively low, varying between 6.5 and 7.8 m^3/t. Due to the geological structure, the gas concentration abruptly rises in three roads of 4,304 working faces, with the most significant level reaching 15.09 m^3/t. Recurrent coal and gas outbursts were observed during excavation, indicating that these issues will intensify as the mine extends toward the west. This poses a substantial risk to the safety and productivity of the mine. The No. 8 coal seam is situated beneath the No. 3 coal seam, exhibiting a reduced gas concentration level and presenting no risk of outbursts. The average separation between the two coal seams measures 37 m. The No. 8 coal seam can act as the safeguarding layer for the No. 3 coal seam, effectively alleviating pressure and providing protection for the No. 3 coal seam.

2. Fracture Development Mechanism of Coal Seam Overlying Strata at Close Distances: A Macroscopic Perspective

The mining process causes a redistribution of the initial stress distribution in the surrounding rocks as the coal seam is extracted. Simultaneously, each layer of superimposed strata likewise undergoes horizontal and vertical displacement. In the caving zone, the layers of rock above undergo separation and subsequent failure, resulting in a fragmented rock mass with numerous voids between the rock blocks. This creates a large fracture zone, facilitating gas accumulation and transport. As coal mining progresses, the fragmented rock mass in the caving zone gradually becomes more compact, with separation continuing at higher elevations [22]. Furthermore, the underlying rock layer undergoes fracturing, resulting in the formation of penetrating fractures. The separation zone, situated above the caving zone, consists mainly of two types of fractures: vertical and oblique crossing tensile fractures and separation fractures along the layer.

2.1. Development Mechanism of Vertical Fractures. During the early phase of coal seam roof collapse induced by mining activities, the rock mass near the coal face frequently cracks, resulting in the formation of well-defined blocks. The rock blocks next to each other are connected by a hinge-like relationship due to a horizontal pushing force. The cracked rock blocks in the wedge-shaped area exhibit characteristics of a voussoir beam structure. If the space available for the suspension of overlaying strata is sufficiently large, surpassing the maximum extent of a specific rock layer, the rock layer will experience fracturing [23]. The fractures along the layer will be vertically fractured and penetrated, creating the upper border of the primary gas flow channel [24].

The strength condition required for fracture deformation is as follows:

$$L_i \geq [L_i] = 2h\sqrt{\frac{[\sigma_{is}]}{3\gamma H}}. \tag{1}$$

In the above equation, σ_{is} is the unidirectional tensile strength of the i-th layer of overlying strata in units of MPa; L_i is the stable span of the i-th layer of overlying strata in units of meters [25].

In addition, the deformation coordination condition should also be satisfied as follows:

$$\begin{aligned} \Delta W_{mi} &= h'_{i+1}\left(K'_p i + 1 - 1\right)\left(1 - \exp\left(-\frac{x}{2l_i}\right)\right) \geq \Delta \\ &= h\left(1 - \sqrt{\frac{1}{3nK\overline{K}}}\right). \end{aligned} \tag{2}$$

In the above equation, m is the coal seam mining height; l_i is the length of rock layer break; K_{pi} is the residual dilatancy

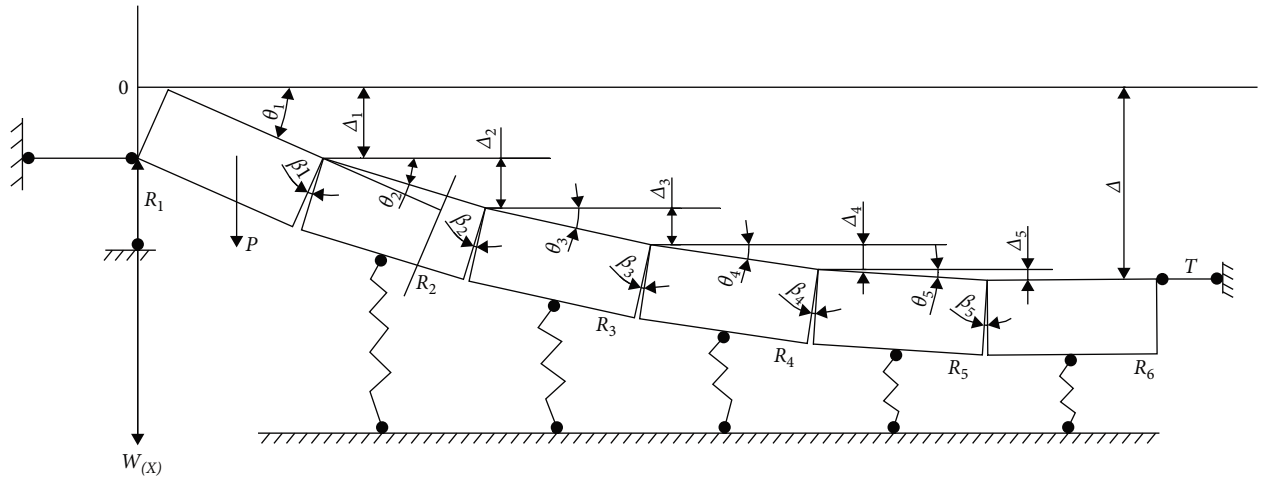

Figure 1: Overlying strata breakage in the fracture zone.

coefficient of the internal rock layer; $\sum h_i'$ is the distance from the i-th group of structures to the coal seam roof; W_{xi} is the displacement curve of the i-th group of structures; $\overline{K}$ is the ratio of compressive strength and compressive strength between rock blocks, K is the state parameters of rock blocks, generally 1/3–1/2.

The deformation coordination condition for beam structure break refers to the condition where shear sliding instability or other structural instabilities are absent. This is based on the equilibrium condition of fractured rock blocks that are stable structurally. Specifically, the maximum allowable sinking depth at the position where each broken rock mass interlocks with each other should be less than the noncoordinated deformation between the adjacent i-th and $i+1$th layers of rock masses.

Based on the results of similarity simulation experiments, the fracture development zone is the area from the contact point between the overlying strata of the gob side and the caving crushed gangue to the coal face breakpoint. Figure 1 shows the overlying structure model, which is composed of multiple adjacent fractured blocks [26].

Let the rotation angle of the i-th broken rock block be θ_i. Then, based on the mutual movement relationship between the rock blocks and the deformation coordination condition, the opening angle of any vertical fracture in a broken block i can be determined as follows:

$$\beta_i = \theta_i - \theta_{i+1}. \tag{3}$$

According to the geometric relationship, $\theta_i = \arcsin \Delta_i / L_i \approx dW/dx$, substituting into Equation (3), we have the following:

$$\beta_i = \frac{dW_i}{dx_i} - \frac{dW_{i+1}}{dx_{i+1}} = \int_{x_i}^{x_{i+1}} W'' dx. \tag{4}$$

From the above equation, it can be seen that the opening angle of the vertical fracture is related to the second derivative of the subsidence curve equation within the rock layer.

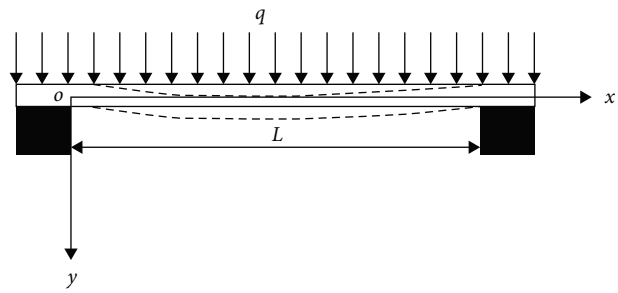

Figure 2: Mechanical structure model of rock beam.

2.2. Development Mechanism of Separation Fractures. The overlying rock mass above the mining face is a composite beam. During the coal mining process, due to the varying bending stiffnesses of beams made from different rock types, different deflections occur during their bending deformation. This results in the formation of separations, with the gaps between these layers being identified as separation fractures. As the working face advances, separation fractures undergo a dynamic development process: generation, development, expansion (fracture), contraction, and closure, moving in tandem with the overlying strata. The height and span of the separation arch increase with the expansion of the mining width and length. Upon reaching a certain threshold, their height and span stabilize, and they only propagate forward with the increasing mining length [27, 28].

A single overlying rock can be simplified as a rock beam [29]. A mechanical model is established to analyze the mechanics of separation development based on the strain of the rock beam. The mechanical structure model of the rock beam is shown in Figure 2.

According to the theory of material mechanics, the approximate differential equation of the deflection curve is as follows:

$$\frac{d^2\omega}{dx^2} = \frac{M}{EI}. \tag{5}$$

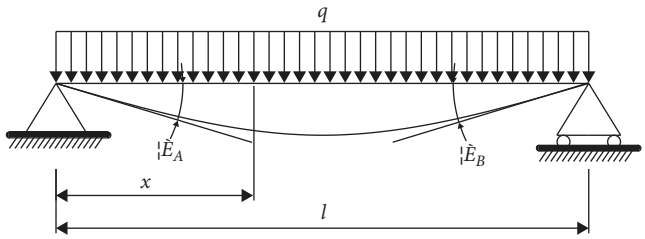

Figure 3: Mechanical model of a simple beam.

Where ω and x are the longitudinal and transverse coordinates of the deflection curve, respectively, M is the bending moment, and E is the modulus of elasticity of the beam [30].

Under small deformation conditions, the deflection curve is relatively flat, and the angle of rotation is small so that we can simplify the above equation as follows:

$$\theta \approx \tan\theta = \frac{d\omega}{dx} = f'(x). \tag{6}$$

Multiplying both sides of Equation (5) by dx and integrating, we get the angle of rotation equation as follows:

$$\theta = \frac{d\omega}{dx} = \int \frac{M}{EI} dx + C. \tag{7}$$

Multiplying both sides by dx and integrating again, we obtain the deflection equation as follows:

$$\omega = \int \int \left(\frac{M}{EI} dx\right) dx + Cx + D. \tag{8}$$

Assuming that the rock beam is a simply supported beam and subjected to uniformly distributed load from the overlying strata, the model is shown in Figure 3.

Calculating the reaction force and bending moment equations of the simply supported beam and substituting into Equation (7), we obtain the following:

$$EI\omega' = -\frac{ql}{4}x^2 + \frac{q}{8}x^3 + C. \tag{9}$$

Substituting this into Equation (8), we get the following:

$$EI\omega = -\frac{ql}{12}x^3 + \frac{q}{24}x^4 + Cx + D. \tag{10}$$

As the deflection at the hinge support is zero,

When $x = 0$, $\omega = 0$; then $D = 0$.

The deflection curve is symmetric with respect to the midpoint of the span, just like the beam's external load and boundary conditions. Therefore, the cross-sectional slope and angle of the tangent (ω') to the deflection curve should be 0 at the midpoint of the span.

When $x = \frac{l}{2}$, $\omega' = 0$; then $C = -ql^3/24$.

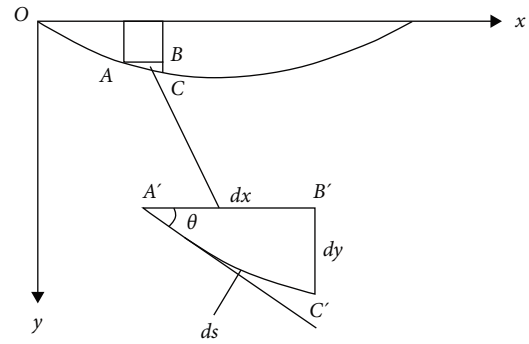

Figure 4: Schematic diagram of curve length differential for rock beam.

Therefore, the equation for the angle of rotation and the deflection curve are as follows:

$$EI\omega' = EI\theta = \frac{ql^3}{24} + \frac{q}{6}x^3 - \frac{ql}{4}x^2 = \frac{q(4x^3 - 6lx^2 + l^3)}{24}. \tag{11}$$

$$EI\omega = -\frac{ql}{12}x^3 + \frac{q}{24}x^4 + \frac{ql^3}{24}x = \frac{qx(x^3 + l^3 - 2lx^2)}{24}. \tag{12}$$

From Equation (12), we can get the extreme value of deflection as follows:

$$\omega\Big|x = \frac{l}{2}\frac{5ql^4}{384EI_{\max}}. \tag{13}$$

In Equation (11), setting $x = 0$ and $x = l$, we can obtain the maximum absolute value of the cross-sectional slope of the angle of rotation, which is the following:

$$\theta A_B \frac{ql^3}{24EI_{\max}}. \tag{14}$$

From Equation (6), when $\omega = y$, the angle of rotation of the beam is $\theta = dy/dx$.

Figure 4 shows the differential diagram of the curve length of a rock beam with a length of l.

From Equation (6), we have the following:

$$dy = \theta dx. \tag{15}$$

From Figure 4, we know that

$$s = \sqrt{(dx)^2 + (dy)^2} = \sqrt{1 + \theta^2}\, dx. \tag{16}$$

Which means that

$$s = \int_0^l \sqrt{(1 + \theta^2)}\, dx. \tag{17}$$

For a simply supported beam,

$$\theta = \frac{dy}{dx} = \frac{q}{24EI_Z}(4x^3 - 6lx^2 + l^3). \tag{18}$$

The curve length S is as follows:

$$S = \int_0^l \sqrt{1+\theta^2}dx = \int_0^l \sqrt{1+\left[\frac{q}{24EI_Z}(4x^3 - 6lx^3 + l^3)\right]^2}dx. \tag{19}$$

The value of S can be calculated using the Newton–Cotes quadrature formula [30]:

$$I(f) = \int_a^b f(x)dx = (b-a)\sum_{k=0}^{n}\left[C_k^{(n)}f(x_k)\right]. \tag{20}$$

Where

$$x_k = a + kh \quad (k = 0, 1, \ldots, n). \tag{21}$$

$$h = \frac{b-a}{n}. \tag{22}$$

$$\begin{aligned} C_k^n &= \frac{h}{b-a}\int_0^n \prod_{\substack{j=0 \\ j\neq k}} \frac{t-j}{k-j}dt \\ &= \frac{(-1)^{n-k}}{n\cdot k!(n-k)!}\int_0^n \prod_{\substack{j=0 \\ j\neq k}} (t-j)dt. \end{aligned} \tag{23}$$

When $n = 3$, the convergence and stability of the above integral are guaranteed [31], then,

$$\int_a^b f(x)dx = \frac{b-a}{8}\left[f(a) + 3f\left[\frac{2a+b}{4}\right] + 3f\left[\frac{2a+b}{4}\right] + f(b)\right]. \tag{24}$$

Therefore, for a simply supported beam, the average strain ε is as follows:

$$\varepsilon = \frac{S-l}{l}. \tag{25}$$

Substituting the curve length S into the above equation and letting $\mu = ql^3/24EI_Z$, we can rearrange the equation to obtain the following:

$$\begin{aligned} \varepsilon &= \frac{S-l}{l} \\ &= \frac{1}{8}\left[2\sqrt{1+\mu^2} + 3\sqrt{1+\left[\frac{11}{27}\right]^2} + 3\sqrt{1+\left[\frac{13}{27}\mu\right]^2}\right] - 1. \end{aligned} \tag{26}$$

If the rock beam fractures, then $\varepsilon \geq [\varepsilon]$, where $[\varepsilon]$ is the maximum strain of the rock beam. Thus,

$$\frac{1}{8}\left[2\sqrt{1+\mu^2} + 3\sqrt{1+\left[\frac{11}{27}\mu\right]^2} + 3\sqrt{1+\left[\frac{13}{27}\mu\right]^2}\right] - 1 \geq [\varepsilon]. \tag{27}$$

We can transform Equation (27) to the following:

$$\frac{1}{8}\left[2\sqrt{1+\mu^2} + 3\sqrt{1+\left[\frac{11}{27}\mu\right]^2} + 3\sqrt{1+\left[\frac{11}{27}\mu\right]^2}\right] \geq 1 + [\varepsilon]. \tag{28}$$

Solving the above inequality, we get the following:

$$\mu \geq \frac{27}{11}\sqrt{\{1+[\varepsilon]^2 - 1\}}. \tag{29}$$

Thus,

$$l \geq \left\{\frac{648EI_Z}{11q}\sqrt{\{1+[\varepsilon]^{-1}\}}\right\}^{\frac{1}{3}}. \tag{30}$$

Thus, if the rock beam that generates separation is a supported beam and its span satisfies Equation (30), the deflection caused by its self-weight will cause the strain to reach the maximum value, and the rock beam will fracture. Under these conditions, the generated separation is considered to have reached the thoroughly mined state.

3. Coal Seam Group Mining Similarity Simulation Platform Construction and Layout of Measurement Points

3.1. Model Construction. Based on the engineering background of the mine's working face and the principle of similarity simulation experiments, appropriate simulation parameters and model sizes were determined.

The geometric similarity parameter α_L was set to 0.01, the bulk density similarity constant a was set to 0.6, and the time similarity constant α_t was set to 1/12. Reasonable layers were determined based on the thickness of each layer. A $2.5 \times 1.5 \times 0.4\,m^3$ 2D mine pressure similarity simulation test system was chosen for the experiment. Each coal and rock layer's similar material mechanics parameters were calculated based on the strength parameters and formulas of different overlying and underlying rock strata, with compressive strength

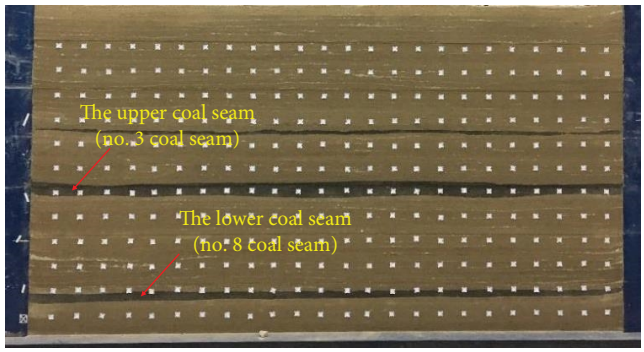

Figure 5: Similar simulation test model.

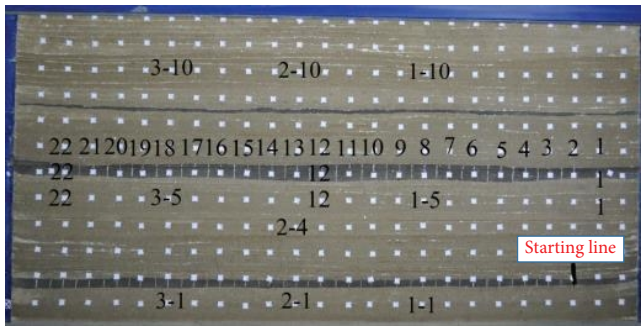

Figure 6: The layout of displacement measuring point.

as the primary index for material ratio selection. For detailed parameters, please refer to the study of Zhang et al. [32] and Wang et al. [33]. The primary materials used in the model include water, gypsum, lime, and fine river sand, mixed in proportion and stirred evenly. Mica powder was added between each layer for precise layering. The model's cumulative height is 140.4 cm, with a total of 62 layers. Hydraulic jacks, instead of overlying load, were used to apply stress to the upper part of the model. A similar experimental model is shown in Figure 5.

3.2. Layout of Measurement Points. To accurately monitor the movement and displacement changes of overlying strata during coal seam advancement, displacement reference points were arranged at different positions on the front of the model. The displacement reference points were arranged in 12 rows and 24 columns with a spacing of 10 cm × 10 cm. First, a column of displacement reference points was arranged in the No. 3 coal seam at a distance of 10 and 7 cm from the left and right boundaries of the model, respectively. Then, a reference point was placed every 10 cm in the upward overlying strata of the No. 3 coal seam and the downward underlying strata of the No. 3 coal seam until both ends of the model, with 288 displacement reference points arranged. A measuring label was pasted and numbered to facilitate observation on each displacement reference point. The actual layout of the displacement reference points is shown in Figure 6.

To simulate and collect the dynamic changes of the overburden pressure and abutment pressure during the mining of the lower protective layer, strain gauge measurement points were arranged at different positions inside the model during its laying process. A total of four layers of strain gauges were arranged in the model, with 15 gauges installed in each layer for a total of 60 measurement points. The specific layer positions are shown in Figure 7, which includes one layer directly above the No. 8 protective layer, two layers between the No. 3 protected layer and the No. 8 coal seam, and one layer on the roof of the No. 3 coal seam. The height of the stress measuring line was 14, 37, 53.8, and 70.4 cm, respectively, measured from 10 cm away from the right boundary and spaced every 15 cm.

3.3. Model Excavation. A 25 cm coal pillar was left on each side of the model to reduce the influence of boundary conditions. According to the time similarity ratio, the face advances by 3.6 cm every 2 hr. First, the lower protective layer of the No. 8 coal seam was mined, and then the No. 3 coal seam was excavated once the overburden was stabilized.

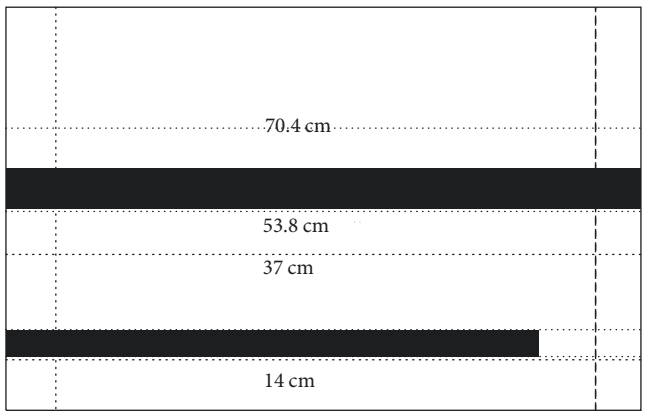

Figure 7: The layout of strain gauges.

3.4. Measuring Instruments and Data Collection. Once the model had dried naturally, the electronic theodolite was used to measure and record each measuring point's horizontal and vertical angles. The DH3816 static strain testing instrument from the China University of Mining and Technology (Beijing) was utilized to gather strain gauge data during the model excavation. Figure 8 displays the measurement tools and data collected. For the experiment, a digital photogrammetry system was arranged on one side. A Canon professional camera was installed on a camera stand, and the focus was adjusted to align with the experimental platform. The electronic theodolite was calibrated for horizontal alignment, and two A8-400 photography lights were used for illumination.

4. Movement, Fracture, and Stress Dynamic Evolution of Overburden

4.1. Collapse Laws of Overburden after Coal Mining. Figure 9 shows the overlying rock movement and dynamic evolution of fractures when the lower coal seam advances at different distances. As the coal seam advances continuously, the suspended area of the roof gradually increases, and the increasing span of the roof causes bending and sinking, resulting in separation fractures between the roof layers. When the working face advances to 45 m, a large roof area collapses, creating

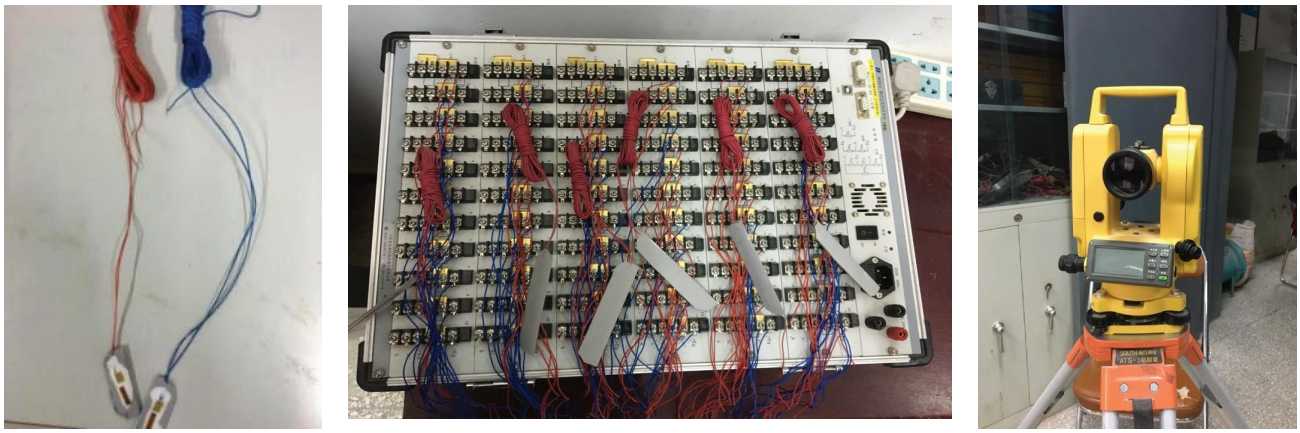

(a) (b) (c)

Figure 8: The measuring instrument for the experiment: (a) strain gauge; (b) DH3816 static strain testing system; (c) electronic theodolite.

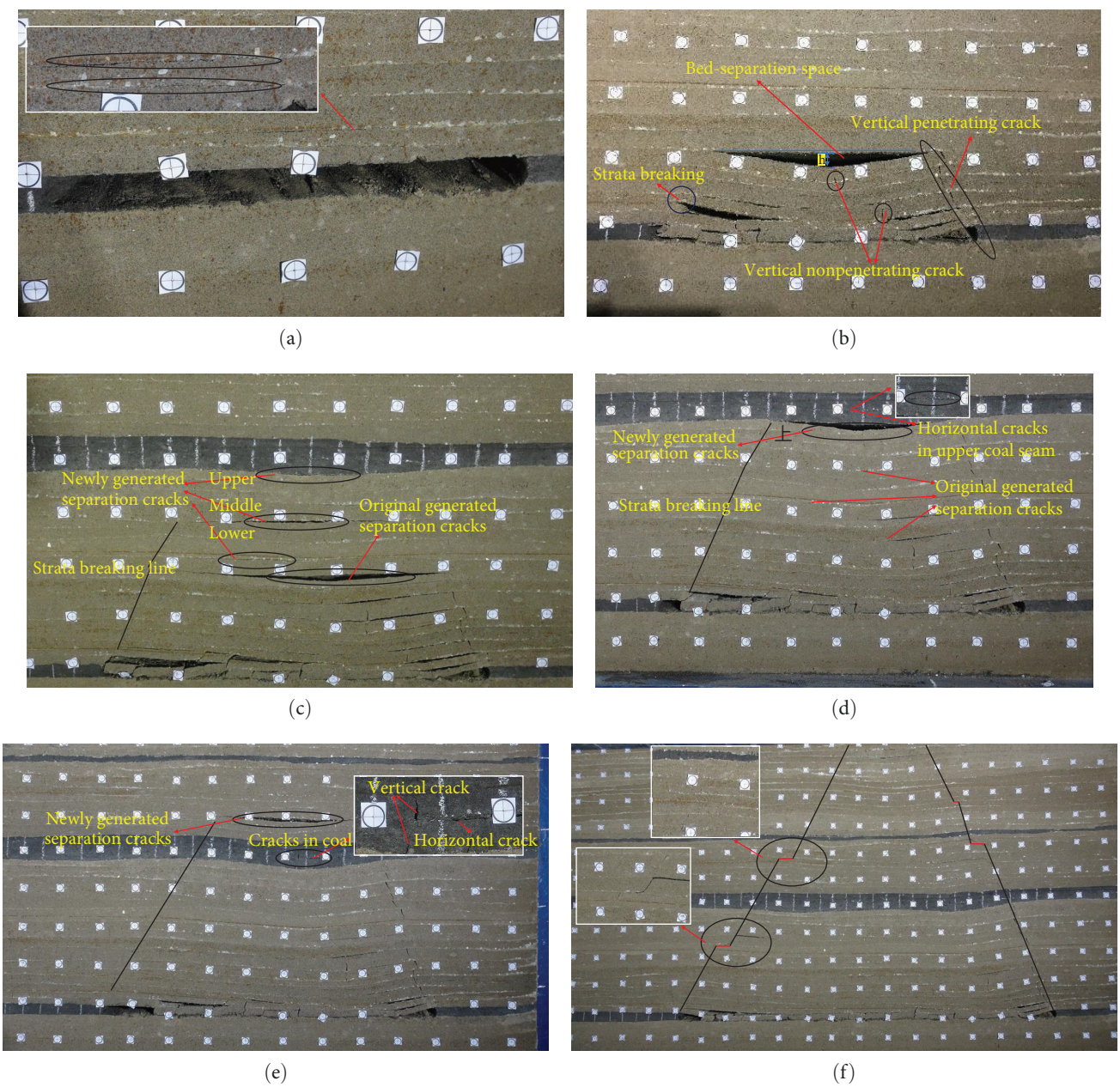

(a) (b) (c) (d) (e) (f)

Figure 9: Dynamic evolution laws of overburden movement and fracture with different distances of lower coal seam advancement: (a) 40 m; (b) 50 m; (c) 75 m; (d) 80 m; (e) 90 m; (f) 140 m.

a significant separation space in the upper part of the roof. The rock layer above loses support, and the separation fractures develop.

When the working face advances to 50 m, the roof of the first layer reaches the ultimate span, breaks through at the working face, and forms an obvious separation fracture with the overburdened rock layer. The rock layer below the base roof also bends, sinks, and fractures due to the breaking of the base roof. Horizontal fractures always occur in the rock layer first; the deflection of the rock layer gradually increases, the width of the horizontal cracks increases, and separation occurs, and then vertical unpenetrated cracks appear in the rock layer. The position of the cutting hole and the rock formation fracture above the working face are inclined toward the direction of the gob. Due to compaction in the middle of the gob, the vertically unconnected fractures do not further develop, and the caving zone presents a prominent trapezoidal area. The upper part of the trapezoid (the upper part of the gob) forms a nonsealed separation space, which is connected to the lower fracture space through vertically connected fractures.

When the working face advances to 60 m, the roof rock layer of the working face forms a hinged structure with the rock layer above the gob area. The surrounding rock bears the roof pressure, the pressure on the support is minimal, and the separation layer crack is up to 18 m.

When the working face continues to advance to 70 m, the overburden continuously moves forward, and the rock layers of the working face roof continue to bend and sink, forming the first periodic weighting with separation fractures in the overburden developing. The original separation fractures are gradually compacted, and new separation fractures develop at higher positions in the top layer. The separation fractures extend to the upper part of the No. 3 coal seam, and the highest separation fracture height reaches 38 m. The coal seam above is affected by the mining activity of the lower coal seam and begins to experience pressure relief and expansion. Hence, a few horizontal fractures appear in the coal seam. New separation layer fissures in the overlying rock continue to develop, the development range of the original separation layer fissures gradually shrinks or even becomes compacted, and the horizontal cracks in the upper coal seam (No. 8) develop significantly.

When the working face continues to advance to 90 m, the overlying rock continues to move forward and upward, the fault line of the rock layer above the working face continues to move forward, and the height of the horizontal cracks in the separation layer exceeds the upper coal seam (No. 3). The highest point of horizontal crack development is approximately 50 m above the roof of the lower coal seam. At the same time, the cracks in the middle of the gob area start to close gradually due to the subsidence and extrusion of the roof. However, the span of the horizontal fractures in the upper No. 3 coal seam increases, and vertical fractures begin to increase, with an expansion of swelling deformation. At this time, influenced by the mining activity of the lower coal seam (No. 8), the pressure relief effect and fracture development of the No. 3 coal seam within a range of about 45 m is good, which is also beneficial to gas desorption and flow. As the working face continues to advance, the separation fractures away from the face side gradually compact or even become slight, and the height of the separation fracture close to the face side further upwardly develops. However, the opening of the fractures becomes smaller. The lower No. 8 coal seam has a small mining height. On the one hand, the volume of the overlying rock layer increases after breaking and sinking. On the other hand, the broken rock in the caving zone gradually compacts, reducing the crushed expansion effect and decreasing the space for overburden movement. When the working face advances to 140 m, the rock break line presents a "stepped" shape.

Figure 10 shows the dynamic evolution of overlying strata movement and fracture during the advancing process of the upper coal seam at different distances. When the upper coal seam advances to a distance of 30 m, the immediate roof hangs and bends down, causing the secondary development of previously closed vertical fractures and horizontal separation fractures in the overlying strata to reopen. Due to the relief effect and fracture development caused by the lower coal seam excavation, the No. 3 coal seam roof exhibits obvious blocky behavior during excavation. When the upper coal seam advances to 40 m, a large roof area collapses, forming a larger space for separation. As the roof forms a voussoir hinge structure, the support only bears a small part of the weight of the overlying strata, and the roof pressure is minimal. However, when the working face advances to 45 m, the range of collapsed overlying strata increases. Although the roof also forms a voussoir hinge structure, due to the accumulation of collapsed overlying layers, the load borne by the support increases, and the mining pressure intensifies, forming the first weighting. Moreover, as the span of the hanging rock layer further increases, the lower part of the rock layer is subjected to tension, resulting in the secondary development of new vertical fractures and previously closed vertical fractures reopening. When the working face advances to 55 m, the height of collapsed overlying strata further increases, and the roof undergoes its first cyclic weighting process, with a step distance of 10 m. The rock mass within the caving zone is more fragmented, and the shattered rock mass at the back of the gob gradually becomes compacted under pressure.

A more stable voussoir beam structure is formed on the roof of the working face side, and when the working face advances to 65 m, the height of the overlying strata separation reaches approximately 30 m, and the pressure borne by the support from the overlying strata increases to somewhat. However, due to the voussoir structure formed by the surrounding rock of the working face, it transfers the overlying strata pressure to the front of the working face and the gob side. When the working face advances to 75 m, the rock mass's voussoir structure loses support from the front coal wall, causing it to break and sink along the breaking line, and most of the load of the overlying strata is transferred to the gob area through a higher voussoir beam structure. The support bears the weight of the upper part of the collapsed rock mass, and the mining pressure intensifies with a step distance of 20 m. When the working face advances to 85 m, the

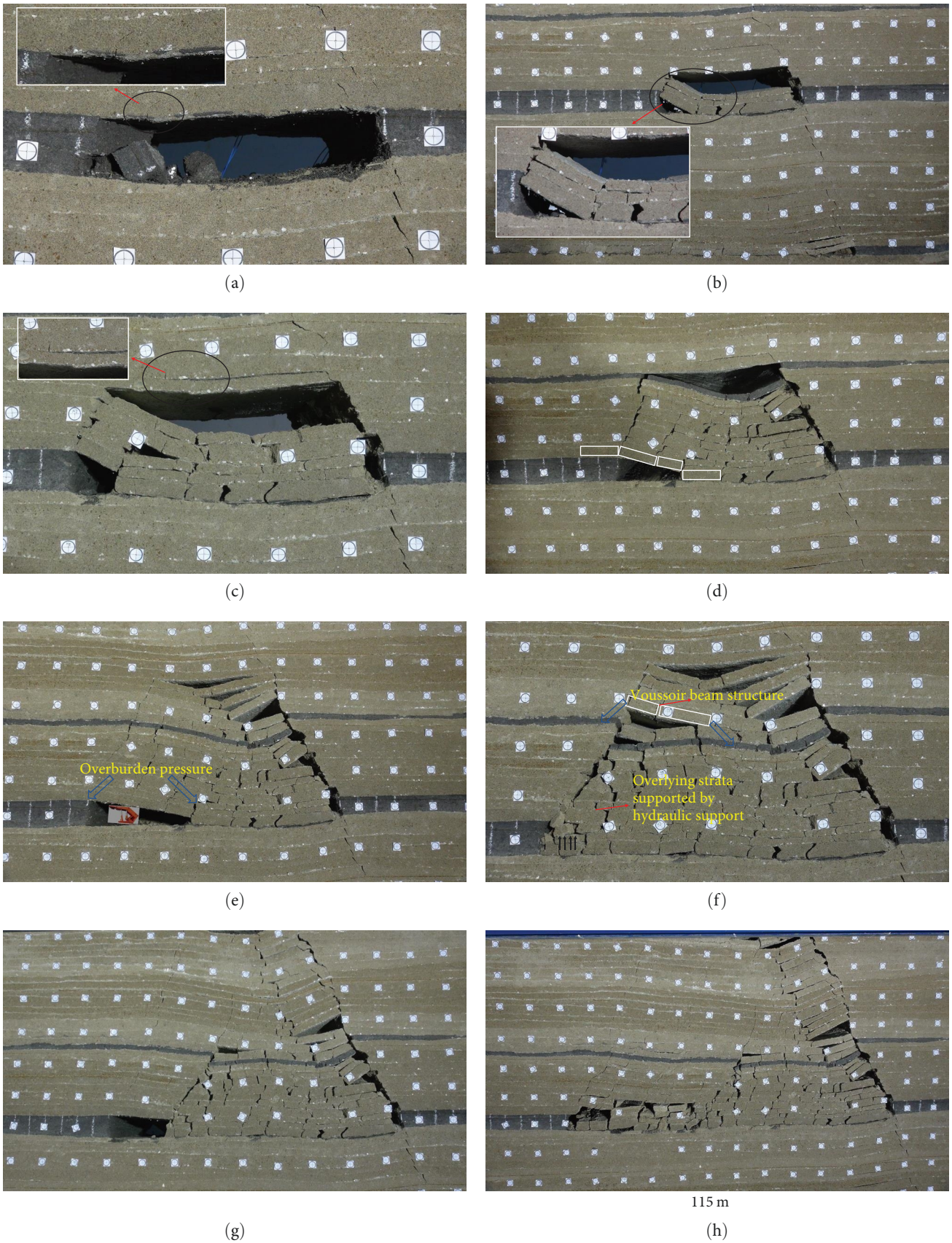

Figure 10: Dynamic evolution laws of overburden movement and fracture with different distances of upper coal seam advancement: (a) 30 m; (b) 40 m; (c) 45 m; (d) 55 m; (e) 65 m; (f) 75 m; (g) 85 m; (h) 115 m.

breaking line of the overlying strata moves forward, and the roof rock layers break and rotary form a structure. The periodic weighting of the working face is not significant, and the height and thickness of the separation in overlying strata increase, with a height of 55 m. When the working face advances to 100 m, the roof rock layer breaks and sinks, causing periodic weighting of the working face with a step distance of 25 m. At this time, three clear rock layer breaking lines are formed in the direction of the face advancing, representing the three-periodic weighting formed by the rotation and sinking of the rock layers. When the working face advances to 115 m, the roof near the working face collapses and forms another periodic weighting with a step distance of 15 m. The stable voussoir beam structure of the overlying strata in the distance from the working face mainly bears the load of the overlying strata, resulting in less intense mining pressure. When the coal seam advances from 115 to 145 m, the roof undergoes rotation and sinking, with a relatively stable overall structure and relatively small amounts of rotation and sinking, gradually easing the mining pressure around the working face. However, when the working face advances to 145 m, the stable structure near the mining area loses balance and collapses, and all the weight is pressed onto the support, causing intense mining pressure on the working face with a step distance of 30 m. When the upper coal seam advances to 165 m, the working face undergoes another periodic weighting with a step distance of 20 m.

4.2. Discontinuity Movement of Upper Coal Seam due to Lower Seam Mining Activity. After the lower coal seam is mined, the displacement change curve of the upper coal seam is shown in Figure 11. Figure 11(a) shows the vertical displacement changes of the three displacement monitoring points of the upper coal seam when the lower coal seam advances at different distances. When the working face advances within 65 m, the displacement changes of the three measuring points are small; the displacement of the 1–6 measuring points is about 8 mm, the displacement of the 2–6 and 3–6 measuring points is almost 0, the 2–6 and 3–6 measuring points are accompanied by the overall overlying rock movement and increase rapidly when the working surface advances 140 and 180 m. When the working surface advances from 75 to 110 m, the displacement of measuring points 1–6 increases rapidly, from 34.3 to 1,570.2 mm. The vertical displacement speed slows down after the working surface advances to 110 m. When the working surface advances to 200 m, the vertical displacement of measuring points 1–6 is about 2,155.9 mm, and the displacement curve almost becomes horizontal, indicating that the subsidence of measuring points 1–6 has approached the maximum value. Figure 11(b) shows the overall displacement curve of the upper coal seam. The vertical displacement in the gob's middle is larger than on both sides. As the gob gradually compacts, the corresponding vertical displacement in the middle of the gob no longer increases.

4.3. Strain Changes of the Floor after Lower Coal Seam Mining. To obtain the changing rules of floor stress during the mining process of the lower coal seam, the floor strain data was effectively extracted and analyzed, and the strain changing rules of three strain gauges 1–6, 1−8, and 1–9 were obtained as the lower coal seam advanced. As shown in Figure 12, it can be seen that the strains at the three measuring points have experienced a process of first increasing to the peak value, then decreasing, and finally stabilizing, indicating that the base plate has experienced pressurization–decompression–pressurization–stabilization during the recovery process since the distance between measuring points 1–6 is 70 m from the cutting face when the working face advances about 190 m, its strain becomes stable, indicating that the stress at measuring points 1–6 has basically returned to the state before mining so that it can be obtained the stress recovery distance in the gob area is approximately 120 m (190−70 m).

4.4. Pressure Relief Rules of the Upper Coal Seam after Mining of the Lower Coal Seam. Through the vertical stress similarity ratio of the model, the strain of the No. 3 stress measuring line is converted into stress, and the stress change pattern of the upper coal seam when the lower coal seam advances at different distances. As shown in Figure 13, when the working face advances 35 m, the maximum pressure relief point is about 14 m behind the working face and 3 m in front of the working face and near the open-off cut area. Stress concentration occurs due to vertical stress transfer. Due to the short advancement distance, the basic roof does not collapse, and the lower coal seam overlying the rock fracture zone has not developed. Therefore, the upper coal seam is less affected by mining, and the stress concentration and pressure relief effect are not significant. The maximum pressure relief point is basically located in the middle of the gob area, and the vertical stress of the upper coal seam is in a "V" shape. As the working face continues to advance, the influence range of protective layer mining gradually increases. When the working face advances to 100 m, the vertical stress in the 5–53 m behind the working face is low, and the pressure relief effect is better. As the roof undergoes periodic collapse and the upper coal seam's pressure relief range and degree continue to increase, when the working face advances to 160 m, the vertical stress distribution of the upper coal seam shows a "W" shape. Due to the support of the collapsed gangue in the gob, the vertical stress in the middle of the gob has recovered to some extent. In summary, during the lower coal seam mining process, the pressure relief degree and range of the upper coal seam gradually increase, the peak point of vertical stress moves forward continuously, and the vertical stress distribution of the upper coal seam changes from "V" type (the immediate roof does not collapse) to "U" type (the immediate roof collapses for the first time) and then to "W" type (the immediate roof undergoes periodic collapse).

5. Pressure Relief Expansion and Crack Evolution Rules of the Upper Protected Coal Seam

During the advancement of the lower coal seam, the pressure relief and expansion deformation of the upper coal seam can be determined by the relative distance changes between

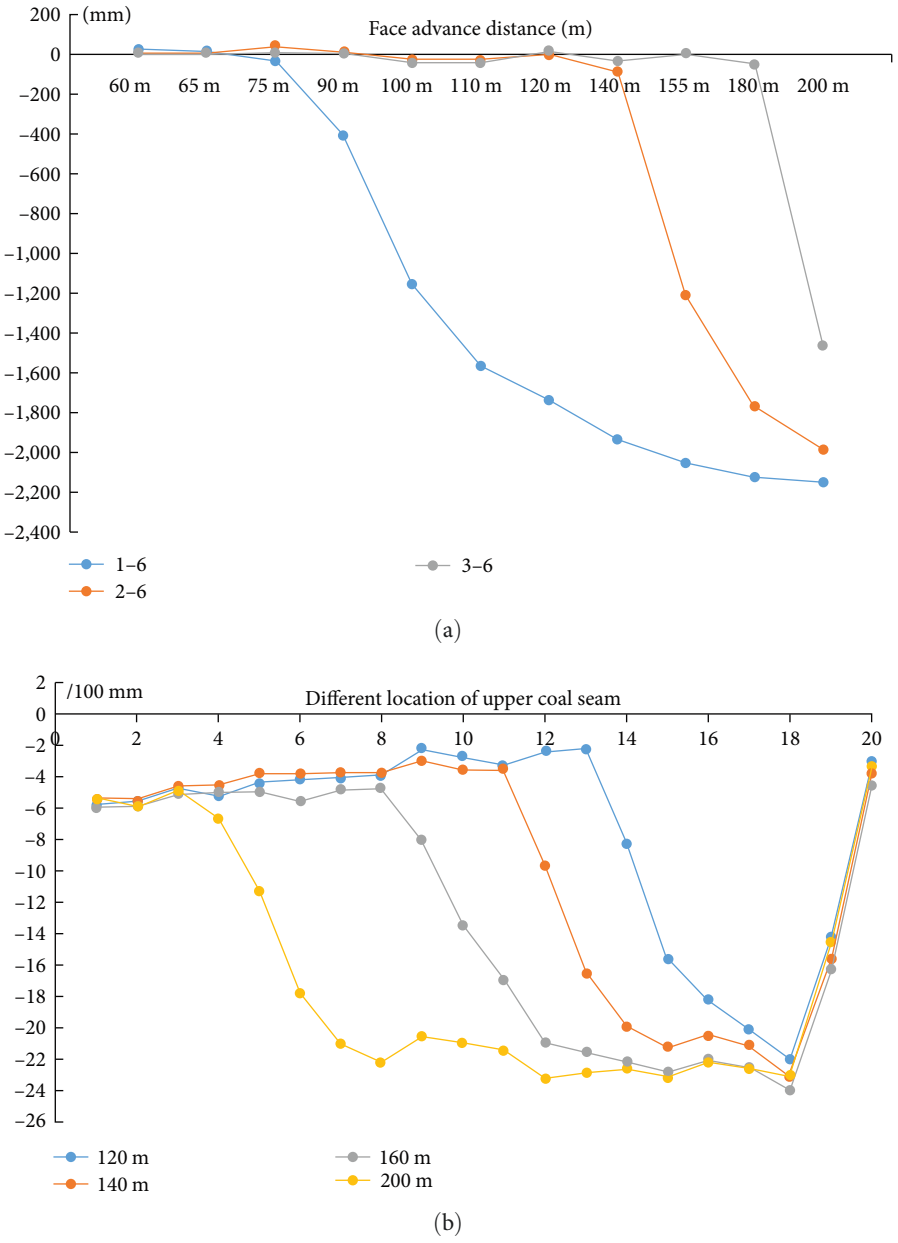

FIGURE 11: Vertical displacement of upper coal seam with different face advance of lower coal seam: (a) vertical displacement of points 1–6, 2−6, and 3–6; (b) vertical displacement of line 4.

points. Assuming the original coordinates of the two points A and B are A ($x0$, $y0$) and B ($x1$, $y1$), respectively, their relative length is $L0$; the coordinates of the two points A' and B' after mining are A' ($x2$, $y2$) and B' ($x3$, $y3$), respectively, and their relative length is $L1$. The specific determination method is as follows:

$$\begin{cases} \dfrac{d_{A'B'}}{d_{AB}} > 1 (a) \\ \dfrac{d_{A'B'}}{d_{AB}} = 1 (b) . \\ \dfrac{d_{A'B'}}{d_{AB}} < 1 (c) \end{cases} \tag{31}$$

If the result satisfies equation (a), it indicates that the two points are in tension; if it satisfies equation (b), it indicates that the two points are not affected by mining; if it satisfies equation (c), it indicates that the two points are under compression.

Using the Data Graph Digitizer software, a coordinate system was established in the images captured by a high-magnification camera, and the coordinates of the displacement monitoring points in the image were extracted to calculate the horizontal and vertical coordinates of the observed monitoring points (upper, middle, and lower points of the upper coal seam) during the advancement of the working face in the lower coal seam. The deformation law of overlying strata, including the upper coal seam's pressure relief and

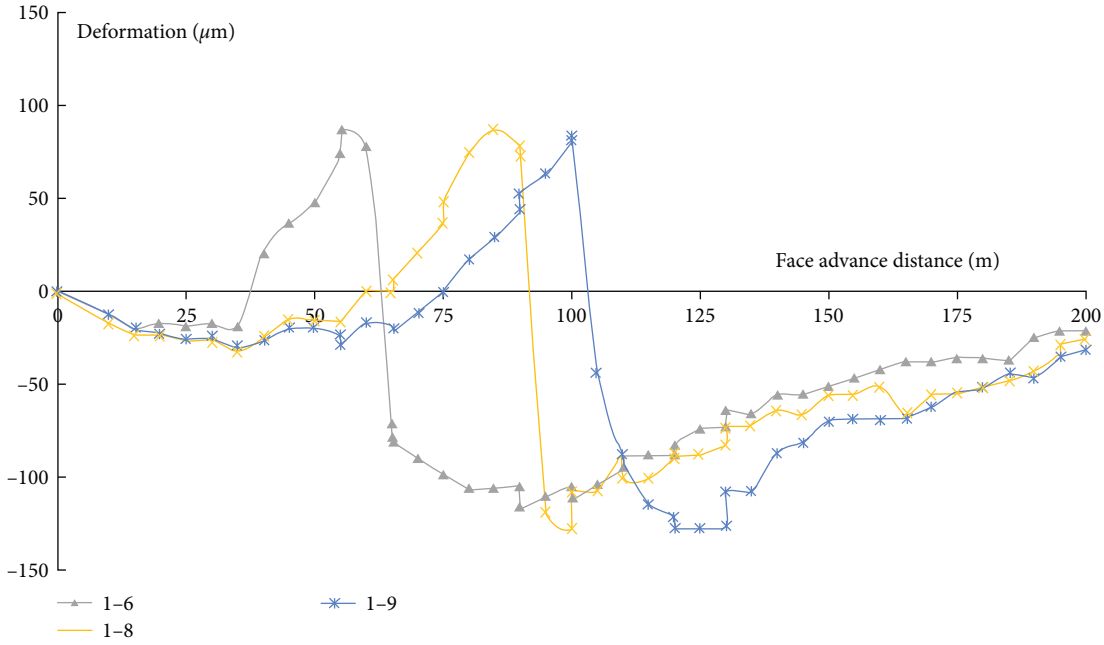

Figure 12: The strain change of measurement points with lower coal seam advancing.

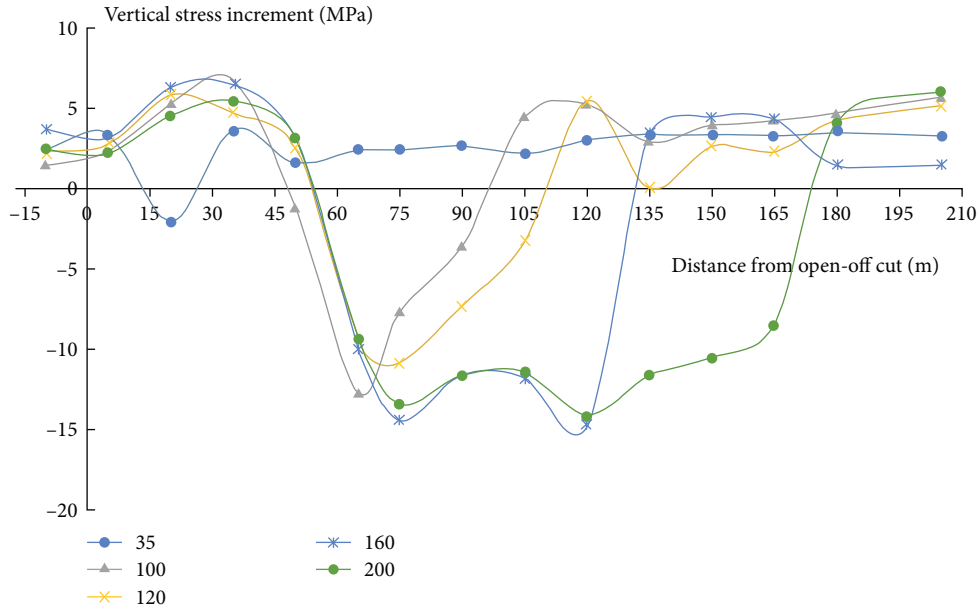

Figure 13: The stress change of the upper coal seam with the lower coal seam advancing.

expansion deformation, was analyzed. The process of extracting the relative coordinates of the monitoring points is shown in Figure 14. The extracted coordinate data are shown in Table 1, and the ratio of relative length between monitoring points at different distances of the advancing working face in the lower coal seam is shown in Table 2.

The curve of the ratio of relative length between the monitoring point in the upper coal seam and the monitoring point in the upper coal seam floor for different face advances of the lower coal seam is shown in Figure 15. Figure 15 shows that the upper coal seam's compression and expansion deformations exhibit similar patterns during the advancement of the lower coal seam but with different distribution ranges. For example, when the working face of the lower coal seam advances 80 m, the No.1 monitoring point in the upper coal seam (10 m from the gob) is located in the compaction zone, where the upper coal seam is under compression, Nos. 2 and 3 monitoring points are in the transitional zone. The upper coal seam between Nos. 4 and 8 monitoring points (20–50 m from the gob) is under tension and experience pressure relief and expansion deformation. The 9th and 10th monitoring points, 60–70 m away from the gob, are in

Figure 14: The measurement of the relative coordinate of the measuring point.

Table 1: The coordinate of measurement points with different face advances of the lower coal seam (part).

	0 m		80 m		90 m		100 m	
	The point in the upper coal seam							
Coordinate	x	y	x	y	x	y	x	y
1	214.108	63.6643	214.155	63.9295	214.413	63.4949	214.38	63.587
2	203.727	63.7489	203.775	63.9214	203.937	63.4949	203.992	63.587
3	193.957	63.6643	194.005	63.829	194.159	63.4949	194.214	63.587
4	184.013	63.7489	184.06	63.9062	184.294	63.6643	184.262	64.0109
5	173.981	63.6643	174.029	63.8985	174.167	63.9182	174.312	65.0283
6	163.601	63.5796	163.561	63.8055	163.69	64.0029	163.662	65.4522
7	153.569	63.6643	153.703	63.8828	153.913	64.5109	153.884	65.1978
8	143.886	63.8336	143.933	63.9602	144.222	64.0029	144.105	64.6891
9	134.029	63.8336	134.076	64.0375	134.27	63.7489	134.239	64.1804
10	124.259	63.7489	124.306	63.945	124.492	63.7489	124.46	63.7565
11	114.663	63.4949	114.711	63.598	114.889	63.4103	114.769	63.4174
12	104.195	63.7489	104.243	63.8446	104.413	63.5796	104.293	63.6717
13	94.6869	63.8336	94.6471	63.8372	94.7222	63.6643	94.6901	63.6717
14	84.9169	63.7489	84.9643	63.8297	85.0317	63.4949	84.9995	63.587
15	75.4086	63.6643	75.456	63.7375	75.5159	63.4949	75.5709	63.587
16	65.2026	63.4949	65.337	63.475	65.3889	63.3256	65.3561	63.3326
17	55.4324	63.6643	55.4798	63.7221	55.6111	63.4103	55.5787	63.5022
18	45.5751	63.8336	45.7098	63.8843	45.746	63.6643	45.6267	63.6717
19	35.2814	64.1722	35.3291	64.2159	35.3571	64.0029	35.326	64.0957
20	26.558	64.4262	26.6059	64.4639	26.627	64.1722	26.5962	64.2652
21	15.916	63.9182	16.0508	63.8614	15.9762	63.6643	16.0316	63.7565
22	4.92446	64.2569	4.97224	64.1925	4.97619	64.0029	4.94507	64.0957

Table 2: The ratio among the relative length of the measuring points with different face advances of the lower coal seam.

Points	80 m Ratio	90 m Ratio	100 m Ratio	120 m Ratio	140 m Ratio	160 m Ratio	180 m Ratio	200 m Ratio
1	0.986227	0.991585	1.001381	0.993012	0.993171	1.001492	0.992976	1.002915
2	1.002746	1.000025	1.018016	1.009878	0.992911	1.001311	1.001159	1.011141
3	1.0113	0.999998	1.00998	1.001623	1.001566	1.002161	1.001644	1.011797
4	1.071452	1.076606	1.061126	1.052325	1.052579	1.060914	1.052489	1.062586
5	1.156053	1.144218	1.052285	1.060857	1.052418	1.069254	1.052369	1.062559
6	1.154608	1.134492	1.026889	1.018321	1.009927	1.009866	1.018314	1.019789
7	1.067335	1.031986	1.017361	1.017442	1.009288	1.001326	0.993215	1.010721
8	1.011698	1.026476	1.045404	1.019023	1.010238	1.01026	1.010237	1.020545
9	0.985278	0.991221	1.010151	1.010492	0.992588	1.001668	0.99267	0.99412
10	0.994169	0.97403	0.992815	1.045553	1.001525	0.992831	0.984029	1.00291
11	0.994537	0.983325	1.001505	1.034967	1.018155	1.009815	1.009837	1.002941
12	0.994242	1.000103	1.001422	1.010063	1.053311	1.018791	1.010396	1.011501
13	1.020056	1.008452	1.018573	1.01858	1.044458	1.03583	1.027175	1.02872
14	0.985861	0.991477	1.001399	0.992908	0.992919	1.009885	1.001407	1.002858
15	1.002897	1	1.001465	0.992892	1.010021	1.027312	1.010145	1.002907
16	1.011309	1.00002	1.018425	1.001472	1.010078	1.018286	1.035378	1.028602
17	0.994203	1.008706	1.010197	0.992877	1.001426	1.001472	1.018891	1.020352
18	1.003143	1.009023	1.009969	1.001725	1.001379	1.001668	1.010021	1.020771
19	1.002867	1.000276	1.001364	0.992785	1.001372	1.001382	0.992518	1.021943
20	0.993742	1.009446	1.001339	1.001419	1.001343	1.001071	1.001448	1.021107
21	1.003254	1.008565	1.001728	1.001842	1.00221	1.001764	1.011009	1.003336
22	1.002854	1.008815	1.010198	1.010276	1.010202	1.019071	1.001841	1.011769

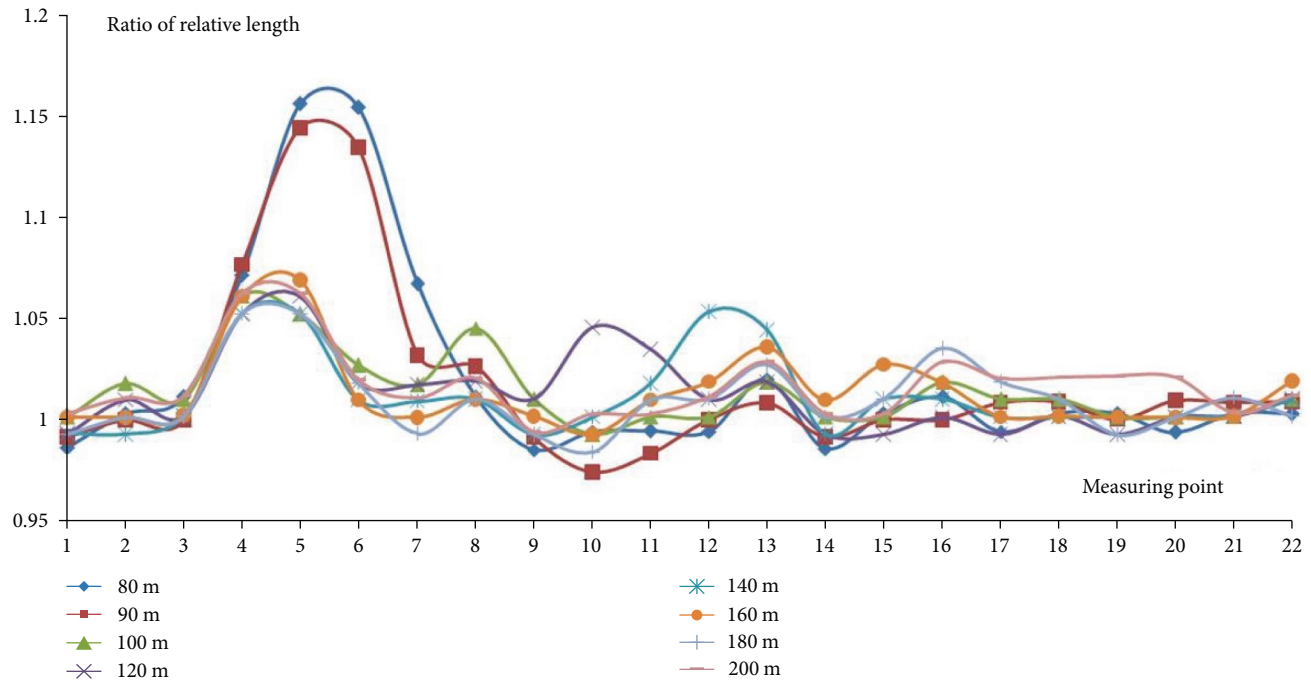

Figure 15: The curve of the relative length of the measuring points with different face advances of the lower coal seam.

the transition zone, while the coal seams beyond 80 m from the gob are less affected by mining activities. As the working face continues to advance, due to sufficient mining, the overlying strata sink as a whole, except for the stretching deformation of the overlying strata at the open-off cut area and the stress and deformation of the upper coal seam in other areas, recover to their premining state.

During the mining of the lower coal seam, Figure 16 shows the dynamic evolution of fractures, pressure relief, and expansion deformation of the upper coal seam. When

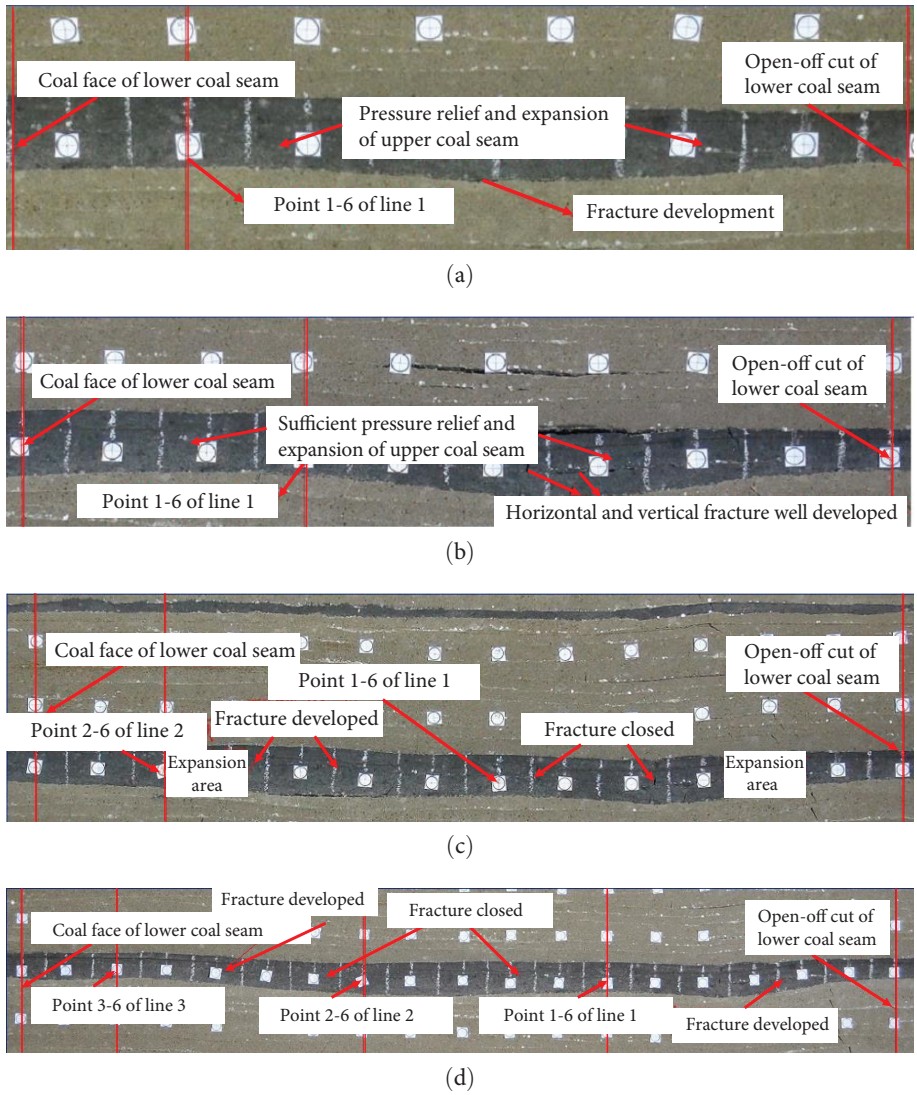

Figure 16: Fracture development and expansion of upper coal seam with different face advance of lower coal seam: (a) 70 m; (b) 90 m; (c) 130 m; (d) 180 m.

the working face of the lower coal seam advances 70 m (Figure 16(a)), the middle part of the upper coal seam in the gob area begins to delaminate with the floor rock layer, and horizontal cracks develop, causing gas desorption from the coal body. When the working face of the lower coal seam advances 90 m (Figure 16(b)), the middle part of the upper coal seam in the gob area is located in the fractured zone caused by mining, and horizontal and vertical cracks are more developed. The upper coal seam's pressure relief and expansion deformation are more sufficient in this area, which is rich in free gas and conducive to gas extraction. When the working face of the lower coal seam further advances 130 m (Figure 16(c)), the fractures of the upper coal seam in the middle of the gob area close due to the compacted collapsed rock mass in the gob area, but the upper coal seam is still under pressure relief state. Corresponding fractures of the upper coal seam develop at the gob and the working face sides of the lower coal seam. As the working face of the lower coal seam continues to advance, the area where fractures of the upper coal seam corresponding to the closed region of the gob area increase, and the pressure relief area becomes stable. When the working face advances 180 m (Figure 16(d)), the closed fracture zone is approximately 90 m, and fractures of the corresponding upper coal seam on the gob side and the working face side of the lower coal seam are in a developed state.

Therefore, based on the pressure relief and fracture evolution laws of the upper coal seam during the mining of the lower coal seam, it can be concluded that any point above the gob undergoes compression, expansion deformation, increased expansion deformation, decreased expansion deformation, and stable expansion deformation phases. After the deformation of the overlying strata above the gob area stabilizes, the upper coal seam can be divided into five zones: compression deformation zone, pressure relief and expansion transition zone, pressure relief and expansion stable zone, pressure relief and expansion transition zone, and compression deformation zone, as shown in Figure 17.

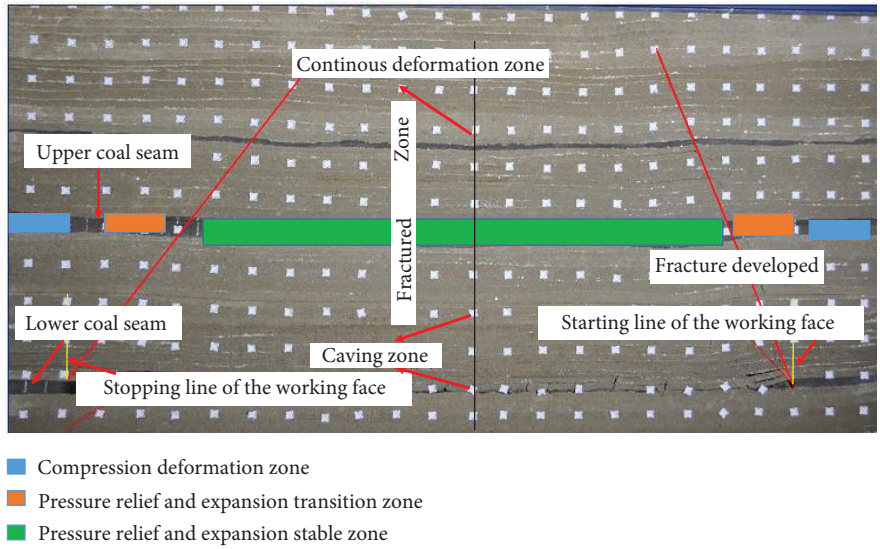

Figure 17: The expansion deformation zone of the upper coal seam after excavation of the lower coal seam.

6. Conclusions

The analysis of roof breakage and overlying strata deformation can provide effective methods for preventing coal and gas outbursts, such as selecting appropriate advancing distances of the working face and setting support parameters reasonably to reduce the impact of mining on the overlying strata and reduce the risk of coal and gas outbursts.

(1) The theoretical derivation of the vertical fracture opening angle formed by the roof breakage should satisfy the fracture deformation strength and coordination conditions. The angle is related to the second derivative of the subsidence curve equation inside the rock formation. Based on the maximum strain theory of a rock beam, the span condition satisfied by the fracture is obtained when the rock beam is regarded as a simply supported beam.

(2) During the advancement of the upper coal seam working face, the roof exhibits large and short periodic weighting lengths and showed the phenomenon of serious and mild periodic weighting, respectively.

(3) The roof periodically collapses and subsides during the advancement of the lower coal seam working face. The pressure relief range and degree on the gob area increase first and then stabilize. The floor experiences a process of increased pressure-reduced pressure-increased pressure-recovery, and the distance for stress recovery in the gob area is approximately 120 m. The extent and range of pressure relief deformation of the upper coal seam continuously increase, and the peak point of vertical stress migrates forward, with the vertical stress distribution form sequentially being "V," "U," and "W."

(4) During the mining of the lower coal seam, the upper coal seam undergoes five stages of compressive deformation, expansion deformation, increased expansion deformation, decreased expansion deformation, and stable expansion deformation, and fractures also undergo development, expansion, and compaction closure processes. After the deformation of the overlying strata above the gob area stabilizes, the upper coal seam can be divided into five zones: compression deformation zone, pressure relief, and expansion transition zone, pressure relief and expansion stable zone, pressure relief and expansion transition zone, and compression deformation zone.

Data Availability

The data used to support the findings of this study are included within the article.

Conflicts of Interest

The authors declare no conflicts of interest.

Authors' Contributions

C.Z. and N.P. conceived the main idea of the paper and designed a similar simulation test model; C.Z. performed a similar simulation model; C.Z., X.C., N.P., S.Z., and M.F. analyzed the data; R.F., A.A., and X.C. contributed analysis tools and theoretical analysis; N.P., C.Z., and A.A. wrote the paper; X.C. and W.Z. did a lot of work to modify figures and proofread the revised version.

Acknowledgments

This paper was supported by the Natural Science Foundation of Jiangsu Higher Education Institutions (no. 20KJB440002), the Blue Engineering Talent Project of Jiangsu Province, and the Foundation of Huaiyin Institute of Technology (no. Z301B20530).

References

[1] C. Zhang, Y. P. Chugh, R. Feng et al., "A numerical investigation of the stress relief zones around a longwall face in the lower seam for gas drainage considerations," *Computer Modeling in Engineering & Sciences*, vol. 127, no. 1, pp. 135–157, 2021.

[2] C. Zhang, J. Wu, C. Wei, Y. Yang, and W. Shen, "Fracture evolution regularity of surrounding rock under different interlaminar strata structure in short-distance coal seams group: a case study in China," *Geotechnical and Geological Engineering*, vol. 39, no. 4, pp. 3193–3206, 2021.

[3] C. Zhang, L. Yu, R. Feng, Y. Zhang, and G. Zhang, "A numerical study of stress distribution and fracture development above a protective coal seam in longwall mining," *Processes*, vol. 6, no. 9, Article ID 146, 2018.

[4] L. Li, G. Wu, and Q. Liu, "Study on overburden movement and fissure evolution law of protective layer mining in shallow coal seam," *Energies*, vol. 15, no. 5, Article ID 1831, 2022.

[5] C. Li, Y. He, X. Sun, and Y. Fu, "Fracture evolution characteristics and deformation laws of overlying strata during the Initial period of longwall mining: case study," *Sustainability*, vol. 15, no. 11, Article ID 8596, 2023.

[6] M. G. Qian, X. X. Shao, and J. L. Xu, *The Oretical Study of Key Stratum in Ground Control*, Publication of China University of Mining and Technology, Xuzhou, 2003.

[7] M. G. Qian and X. X. Shao, "The oretical analysis on the structural form and stability of overlying strata in longwall mining," *Chinese Journal of Rock Mechanics and Engineering*, vol. 14, no. 2, pp. 97–106, 1995.

[8] M. Qian and J. Xu, "Study on the "O-SHAPE" circle distribution characteristics of mining-induced fractures in the overlaying strata," *Journal of China Coal Society*, vol. 23, no. 5, pp. 466–469, 1998.

[9] J. L. Xu, M. G. Qian, and H. W. Jin, "Study on, coal and coal-bed methane simultaneous extraction, technique on the basis of strata movement," *Journal of China Coal Society*, vol. 29, no. 2, pp. 129–132, 2004.

[10] L. Yuan, "Theory of pressure-relieved gas extraction and technique system of integrated coal production and gas extraction," *Journal of China Coal Society*, vol. 34, no. 1, pp. 1–8, 2009.

[11] P. Lu, L. Yuan, and H. Cheng, "Theory and experimental studies of enhanced gas drainage in the high-gas face of low permeability coal multi-seams," *Journal of China Coal Society*, vol. 35, no. 4, pp. 580–585, 2010.

[12] S. G. Li and H. F. Lin, "Model experiment analysis of distribution features of mining fissure elliptic paraboloid zone," *Coal*, vol. 17, no. 2, pp. 19–21, 2008.

[13] H. F. Lin, S. G. Li, and L. H. Cheng, "Experimental analysis of dynamic evolution model of mining-induced fissure zone in overlying strata," *Journal of Mining & Safety Engineering*, vol. 28, no. 2, pp. 298–303, 2011.

[14] H. P. Xie, G. M. Yu, and L. Yang, "Research on the fractal effects of crack network in overburden rock stratum," *Chinese Journal of Rock Mechanics and Engineering*, vol. 18, no. 2, pp. 147–151, 1999.

[15] G. Yu, H. Xie, J. Zhoa, and L. Yang, "Fractal evolution of a crack network in overburden rock stratum," *Discrete Dynamics in Nature and Society*, vol. 5, Article ID 181040, 6 pages, 2000.

[16] J. Liu, T. Yang, L. Wang, and X. J. Chen, "Research progress in coal and gas co-minming modes in China," *Energy Science & Engineering*, vol. 8, no. 9, pp. 3365–3376, 2022.

[17] L. Zhang, Z. H. Kan, and J. H. Xue, "Experimental study on permeability and porosity evolution of sandstone under cyclic loading and unloading," *Chinese Journal of Rock Mechanics and Engineering*, vol. 40, no. 12, pp. 2487–2499, 2021.

[18] Z. H. Cheng, Q. X. Qi, and H. Y. Li, "Evolution of the superimposed mining induced stress-fissure field under extracting of close distance coal seam group," *Chinese Journal of Rock Mechanics and Engineering*, vol. 40, no. 12, pp. 2487–2499, 2016.

[19] Q. Y. Wu, C. W. Guo, and H. L. Zhai, "Physical simulation on spatial distribution of void fraction in overburden due to repeated mining in North Shaanxi mining area," *Coal Science and Technology*, vol. 50, no. 1, pp. 105–111, 2022.

[20] Y. W. Li, Y. J. Zhang, and J. Xiao, "Development law of overburden failure height under repeated mining in multiple coal seams," *Coal Engineering*, vol. 54, no. 7, pp. 97–103, 2022.

[21] H. Lin, L. Li, S. Li, and Y. Ding, "Experimental study on evolution law of pressure relief gas storage and transportation area of repeated mining in coal seam," *Journal of Xi 'an University of Science and Technology*, vol. 41, no. 3, pp. 385–393, 2021.

[22] H. Wagner, "Deep mining: a rock engineering challenge," *Rock Mechanics and Rock Engineering*, vol. 52, no. 5, pp. 1417–1446, 2019.

[23] Y. Xiong, D. Kong, Z. Wen, G. Wu, and Q. Liu, "Analysis of coal face stability of lower coal seam under repeated mining in close coal seams group," *Scientific Reports*, vol. 12, no. 1, Article ID 509, 2022.

[24] J. Zeng, W. Li, J. Liu et al., "Analytical solutions for multi-stage fractured shale gas reservoirs with damaged fractures and stimulated reservoir volumes," *Journal of Petroleum Science and Engineering.doi*, vol. 187, Article ID 106686, 2020.

[25] H. T. Liu, N. J. Ma, and J. Li, "Evolution and distribution characteristics of roof shallow fracture channel," *Journal of China Coal Society*, vol. 37, no. 9, pp. 1451–1455, 2012.

[26] H. P. Xie, B. Q. Lin, and H. W. Zhou, *Theory and Technology of Deep Coal and Gas Co-mining*, Science Press, Beijing, 2017.

[27] D. Liu, S. Wang, and L. Li, "Investigation of fracture behaviour during rock mass failure," *International Journal of Rock Mechanics and Mining Sciences*, vol. 37, no. 3, pp. 489–497, 2000.

[28] H. Mohammadi and S. Pietruszczak, "Description of damage process in fractured rocks," *International Journal of Rock Mechanics and Mining Sciences*, vol. 113, pp. 295–302, 2019.

[29] S. H. Wang, Y. F. Gao, and Z. L. Fu, "Study on classifying and mechanics mechanism of grouting overlying bed-separations developing," *Chinese Journal of Solid Mechanics*, vol. S1, pp. 164–168, 2006.

[30] H. W. Liu, *Mechanics of Material*, pp. 275–282, Higher Education Press, Beijing, 1992.

[31] W. P. Yuan, L. M. Zhang, and X. Q. Huang, *Numerical Analysis*, pp. 275–282, Southeast University Press, Nanjing, 1992.

[32] C. Zhang, Y. Zhang, J. Zuo, and S. Gao, "Fracture pattern of overlying strata in multiple coal seam mining in a physical model vis-à-vis MATLAB analysis and geological radar," *Mining, Metallurgy & Exploration*, vol. 38, no. 2, pp. 897–911, 2021.

[33] B. Wang, D. Zhou, J. Zhang, and B. Liang, "Research on the dynamic evolution law of fissures in shallow-buried and short-distance coal seam mining in Lijiahao Coal Mine," *Scientific Reports*, vol. 13, no. 1, Article ID 5625, 2023.